Electronic Supplementary Information

Sacrificial Zn Strategy Enables Anchoring of Metal Single Atoms on the Exposed Surface of Holey 2D Molybdenum Carbide Nanosheets for Efficient Electrocatalysis

Zongkui Kou[*], *Wenjie Zang, Wei Pei, Lirong Zheng, Si Zhou*[*], *Siwen Zhang, Lei Zhang, John Wang*[*]

Chemicals

Cobalt nitrate hexahydrate ($Co(NO_3)_2 \cdot 6H_2O$; ≥99.0%), nickel nitrate hexahydrate ($Ni(NO_3)_2 \cdot 6H_2O$; ≥99.0%), copper nitrate hexahydrate ($Cu(NO_3)_2 \cdot 3H_2O$; ≥99.0%), Zinc nitrate hexahydrate ($Zn(NO_3)_2 \cdot 6H_2O$; ≥99.0%), 2-methylimidazole (2-mIm; 99.0%), ammonium molybdate ($(NH_4)_6Mo_7O_{24} \cdot 4H_2O$, 99.0%) were purchased from Sigma-Aldrich Co., Ltd. and directly used without any purification. The DI water with the resistivity of 18.25 MΩ cm^{-1} was purified with a water ultrapure cation system.

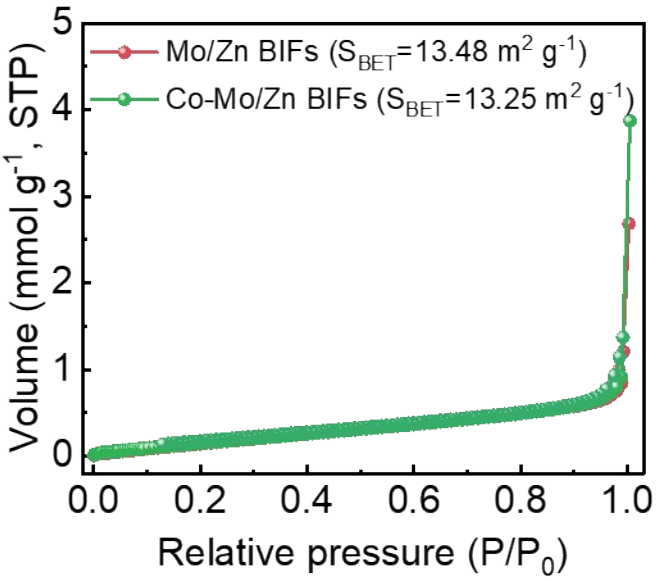

Figure S1. N_2 adsorption-desorption curves of Mo/Zn BIFs and Co-Mo/Zn BIFs.

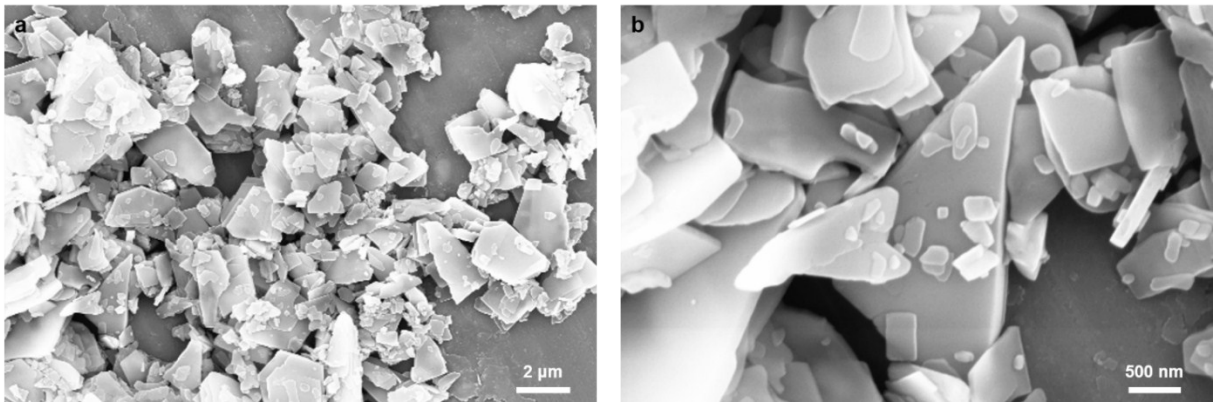

Figure S2. SEM images of Mo/Zn BIFs nanosheets.

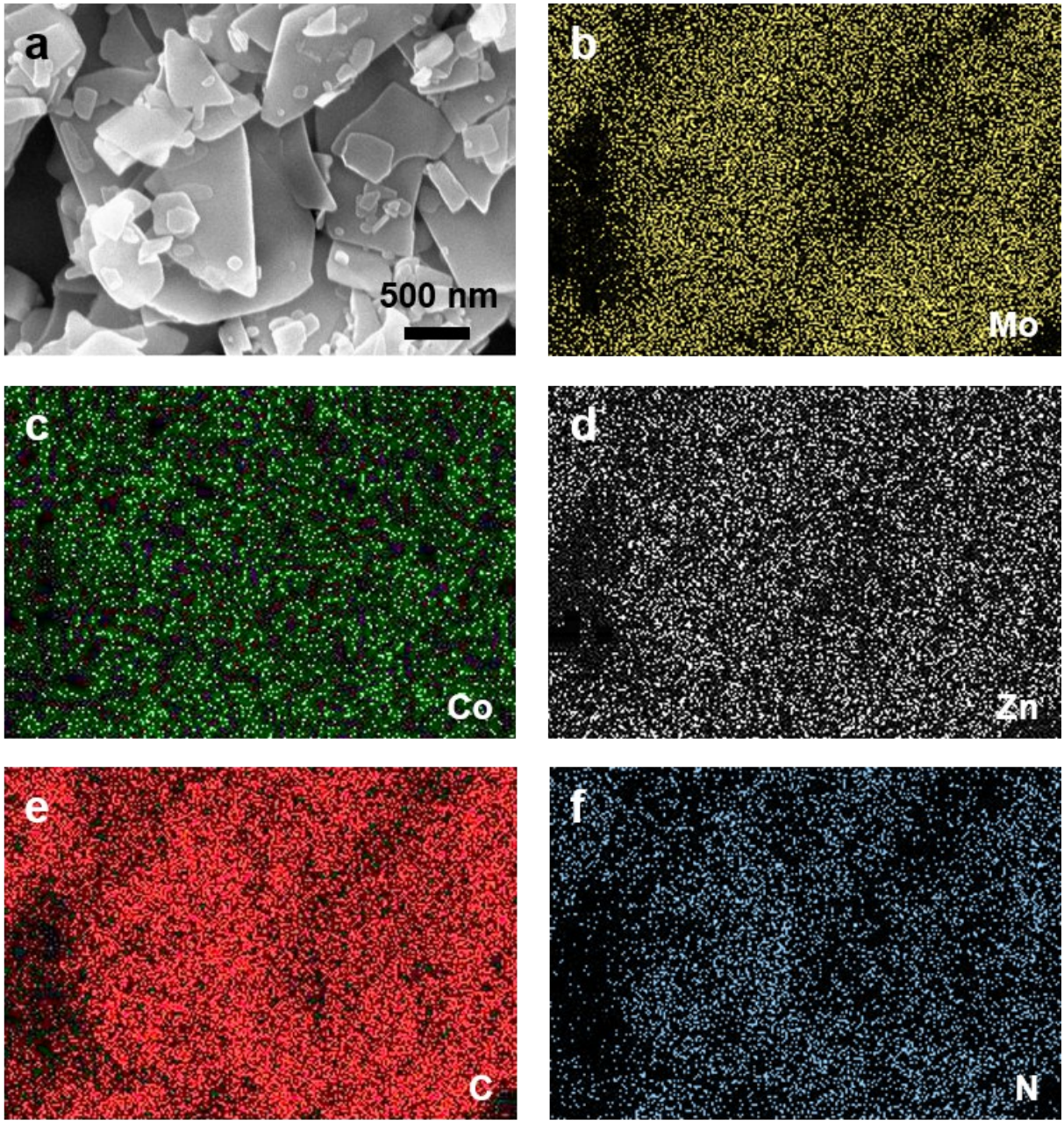

Figure S3. SEM image (a) and elemental mapping (b-f) of Mo/Zn BIFs nanosheets.

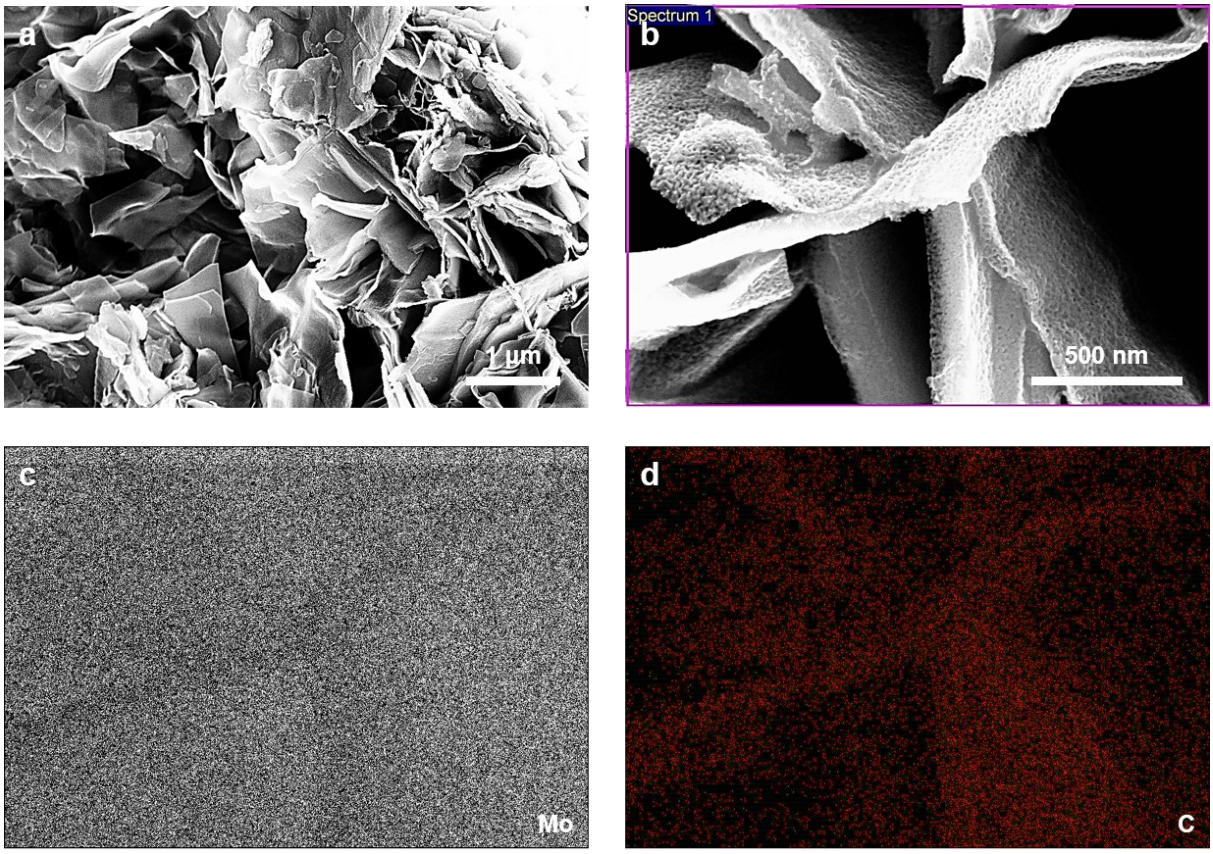

Figure S4. SEM image (a, b) and elemental mapping (c, d) of holey 2D Mo_2C derived from Mo/Zn BIFs nanosheets.

As shown in **Figure S4a**, the as-derived Mo_2C present a typical nanosheet structure, which is consisting of nanocrystal arrays with hexagonal crystal form (see **Figure S5**). The Mo_2C nanosheet also display a holey structure with the irregular holey shape (**Figure S4b**). Mo and C are uniformly distributed across the nanosheet according to Mo and C EDS mapping (**Figures S4c** and **d**).

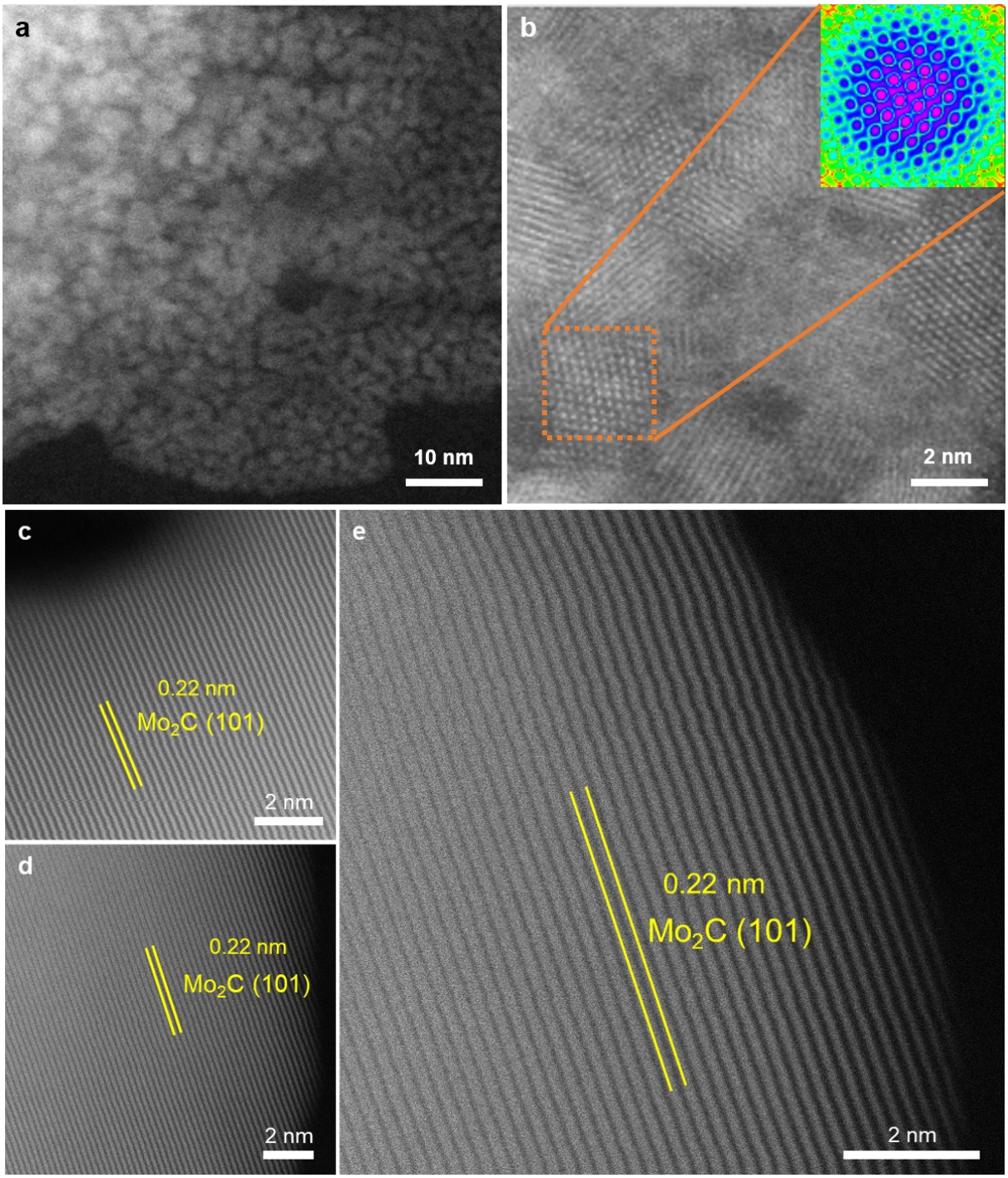

Figure S5. STEM image (a) and high-resolution STEM image (b) of holey 2D Mo_2C. The inset in b is atom-level STEM image, which shows the uniformly hexagonal distribution of bright Mo atoms. High resolution TEM images (c-e) of the Mo_2C kernel in Co SAs/Mo_2C.

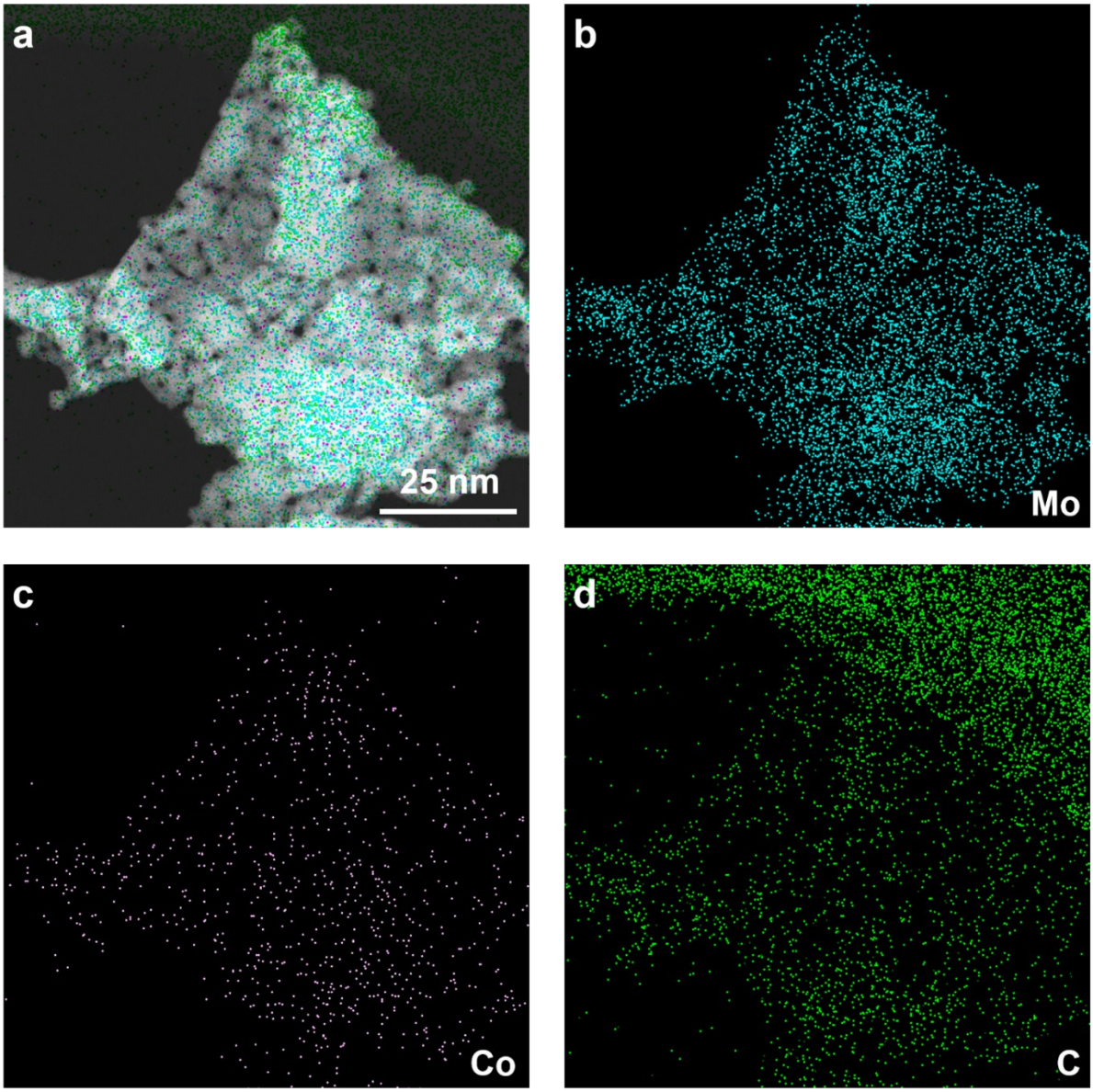

Figure S6. EDS chemical maps of Co SAs/Mo_2C.

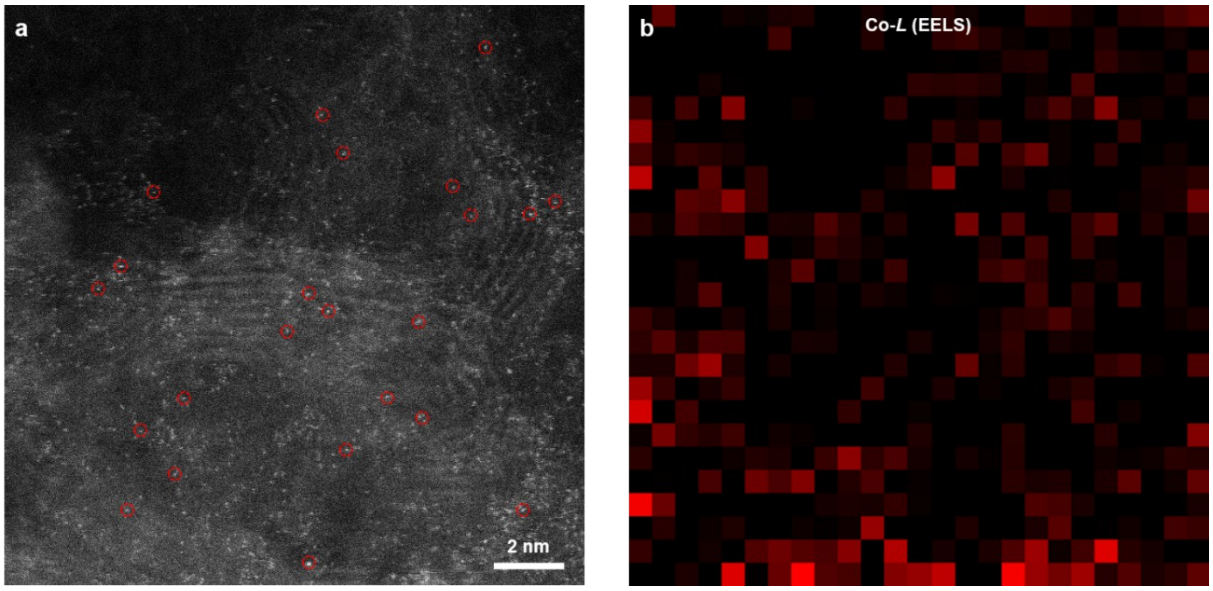

Figure S7. HAADF-STEM image and the corresponding Co-L EELS mapping of Co SAs/N-C. A plenty bright dots can be seen in STEM image of Co SAs/N-C, which is assigned to Co single atoms confirmed by Co-*L* EELS mapping.

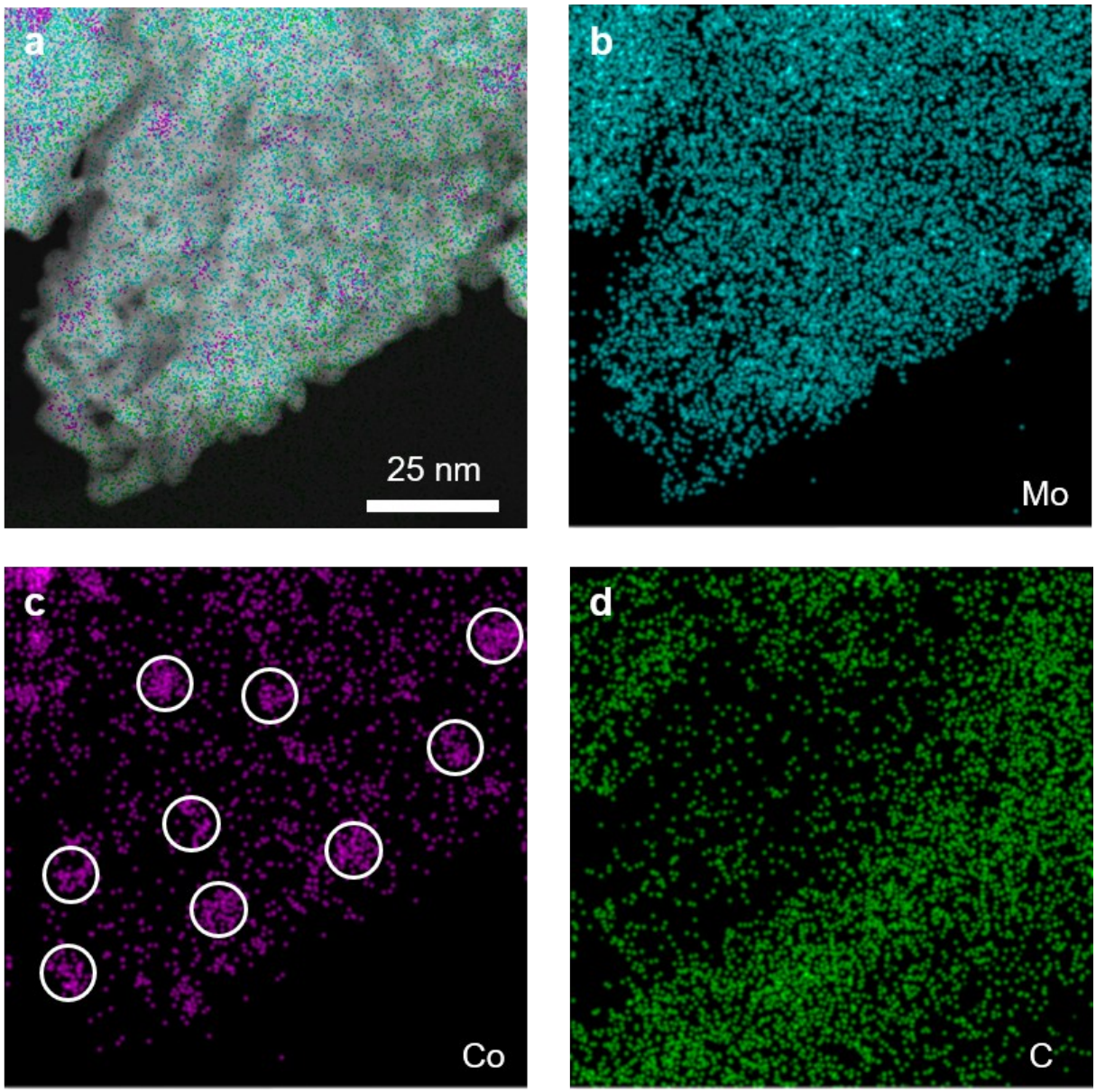

Figure S8. HAADF-STEM image and the corresponding EDS mapping of Co, Mo and C in Co NPs/Mo_2C. By increasing the Co adding amount in the synthesis of Co-Mo/Zn BIFs, Co nanoparticle coupled on Mo_2C can be easily derived. Clearly, Mo and C uniformly distribute on the nanosheet while Co atoms aggregate together to become nanoparticles.

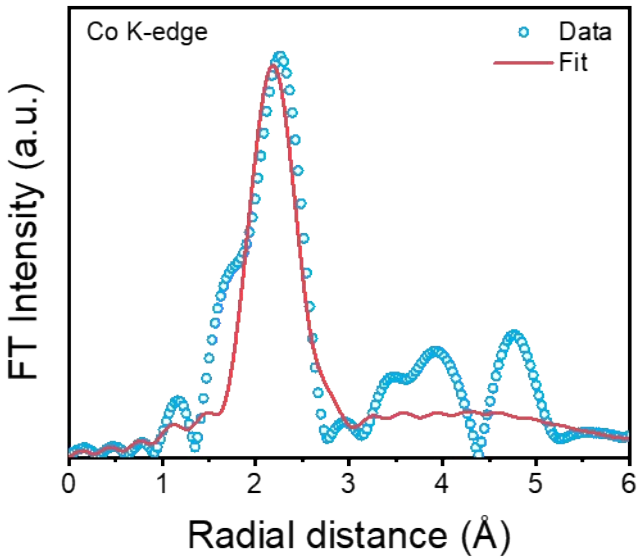

Figure S9. Radial distribution of Fourier-transformed EXAFS signal of Co SAs/Mo_2C with a Co-Co path at R = 2.1 Å.

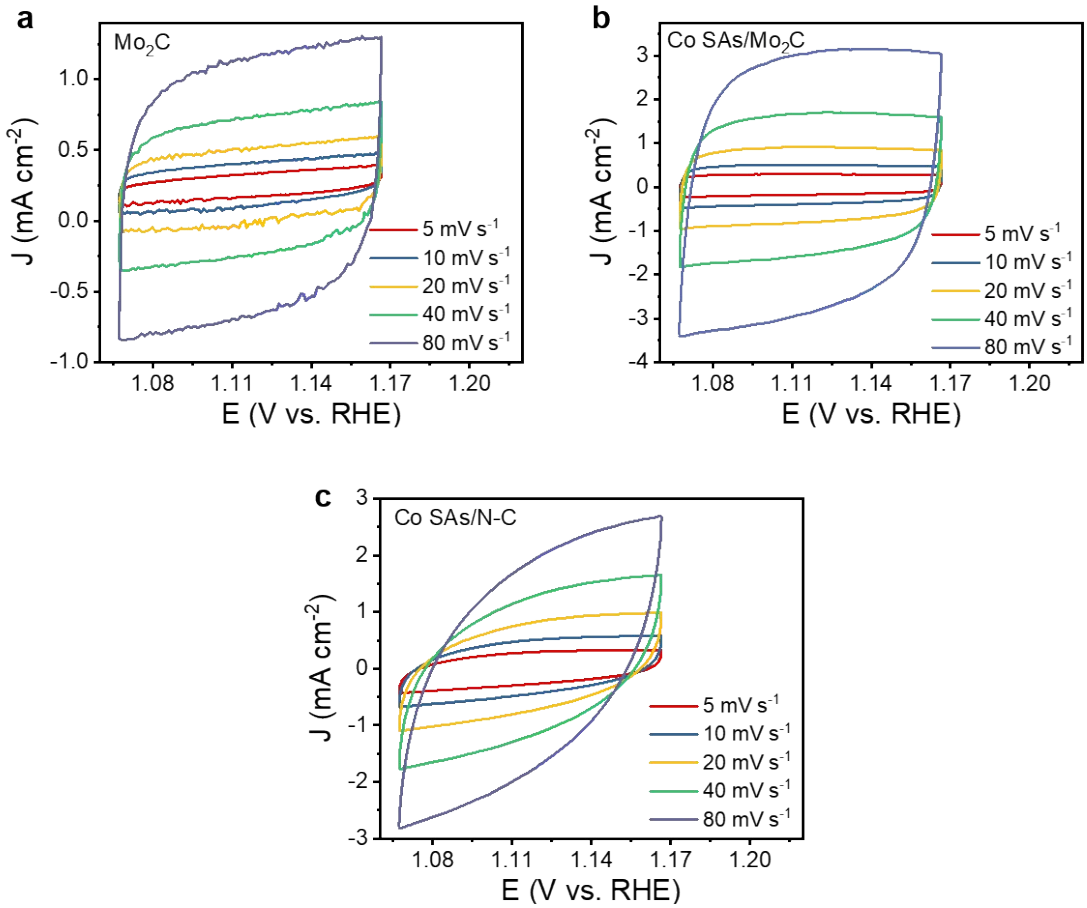

Figure S10. CV curves of Mo_2C, Co SAs/Mo_2C and Co SAs/N-C at the varied scan rates.

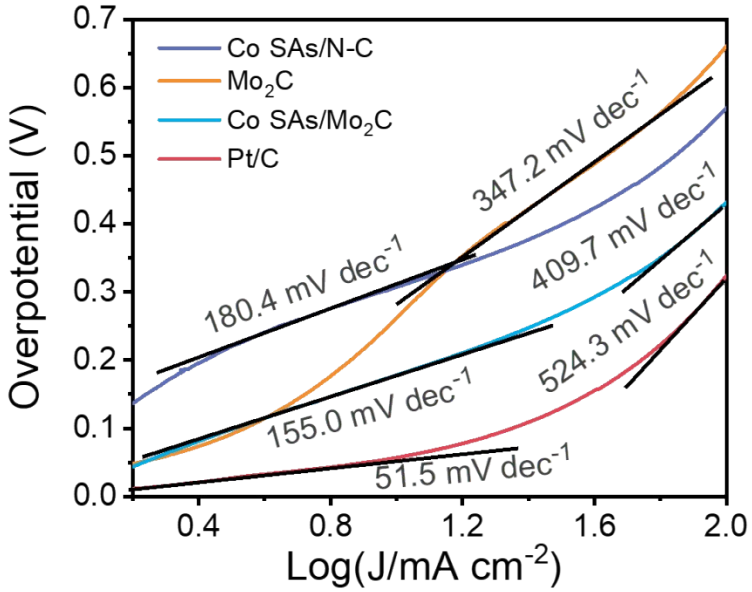

Figure S11. The Tafel curves with calculated slope values derived from the corresponding LSV curves in **Figure 3g**.

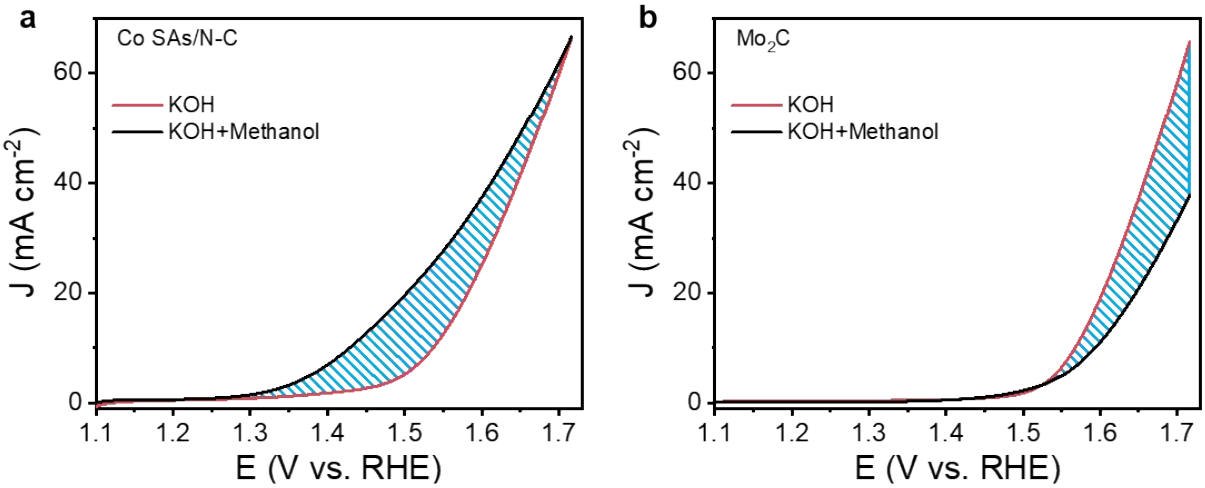

Figure S12. Comparison of LSV curves with or without 1 mL methanol: (a) Co SAs/N-C; (b) Mo_2C. The shaded zone is used to calculate the DLA value.

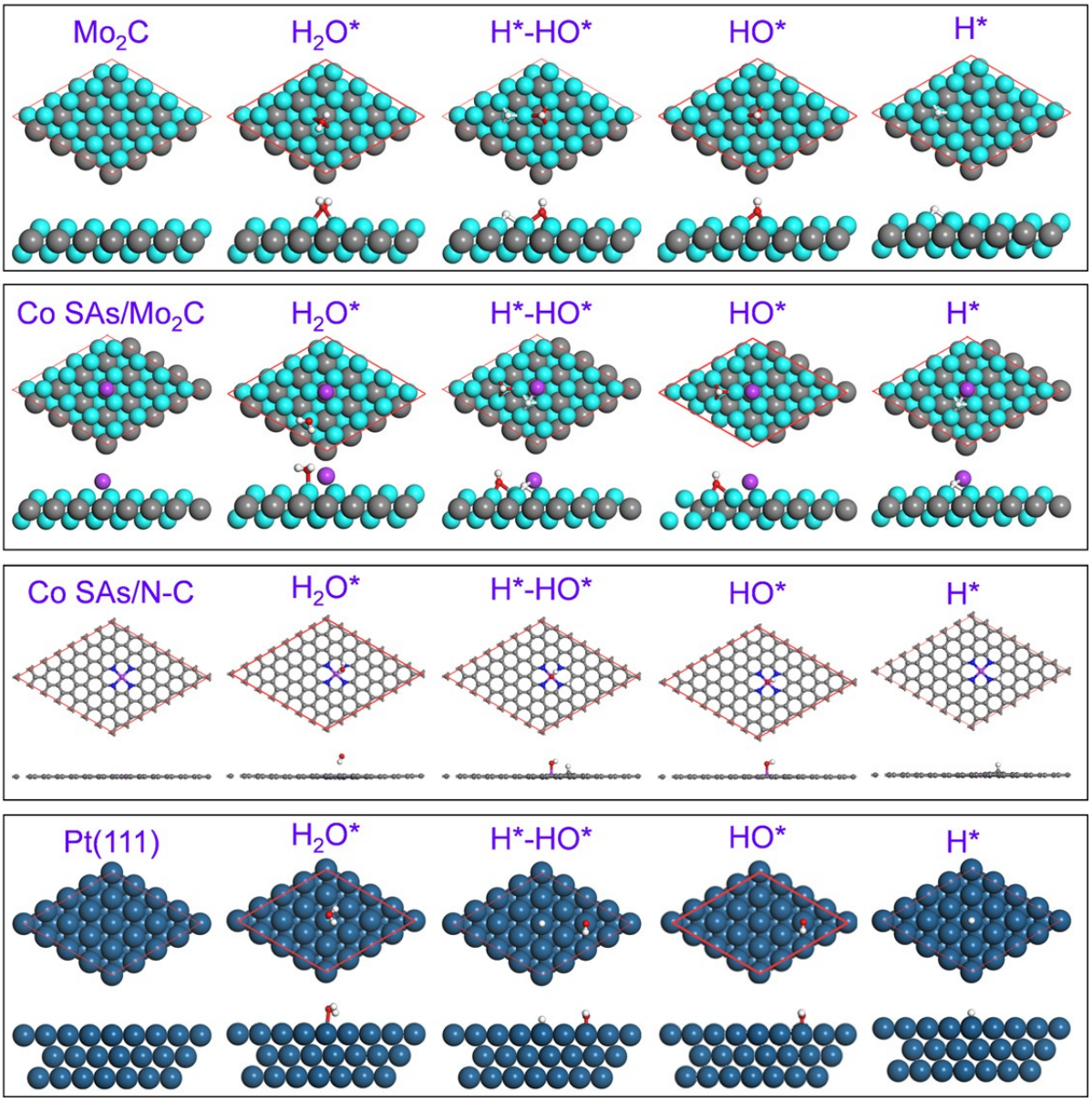

Figure S13. Model structures of (from top to bottom) Mo_2C, Co SAs/Mo_2C, Co SAs/N-C and Pt, and adsorption of various reaction intermediates on each model. The H, C, N, O, Co, Mo and Pt atoms are shown in white, grey, blue, red, purple, cyan and navy blue, respectively. The red boxes indicate the lateral dimension of supercells for calculations.

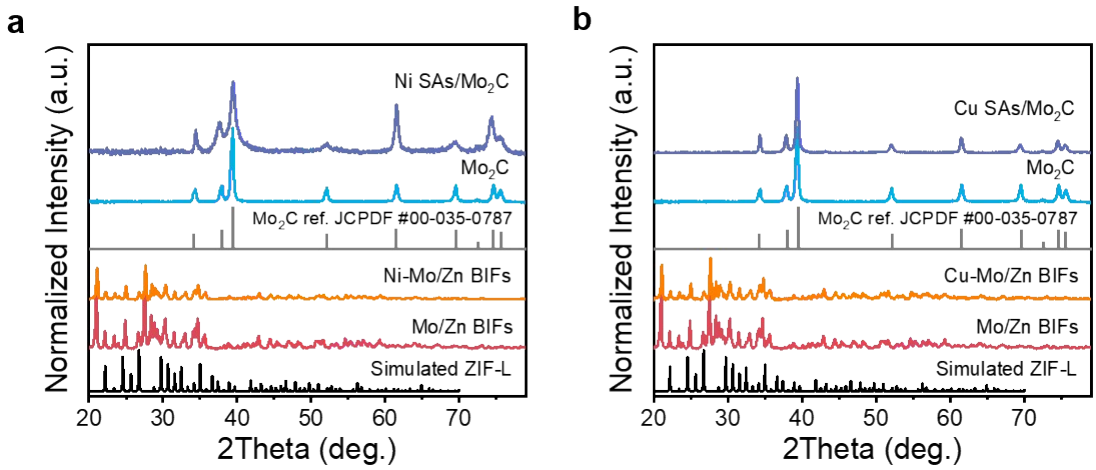

Figure S14. XRD patterns of Ni SAs/Mo_2C and Ni-Mo/Zn BIFs, Cu SAs/Mo_2C and Cu-Mo/Zn BIFs. Simulated ZIF-L, Mo/Zn BIFs and Mo_2C are used as references.

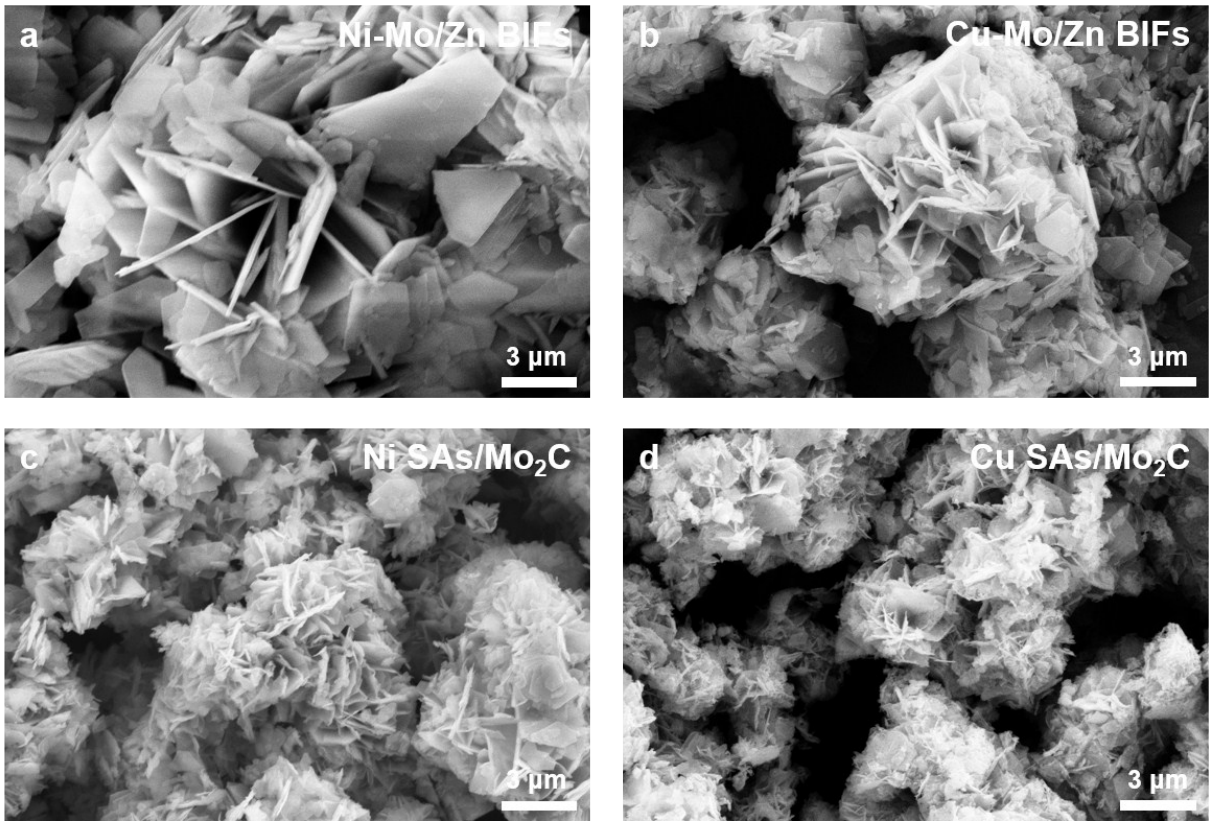

Figure S15. SEM images of Ni-based and Cu-based precursors (a, b) and products (c, d).

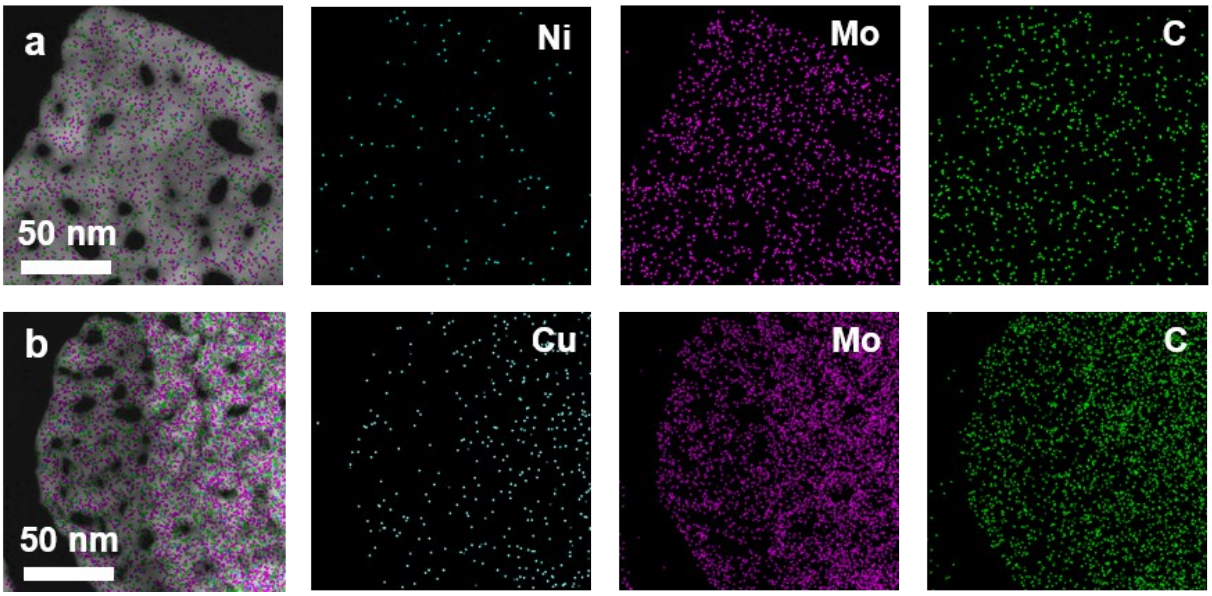

Figure S16. STEM images and the corresponding EDS mapping of Ni SAs/Mo_2C (a) and Cu SAs/Mo_2C (b).

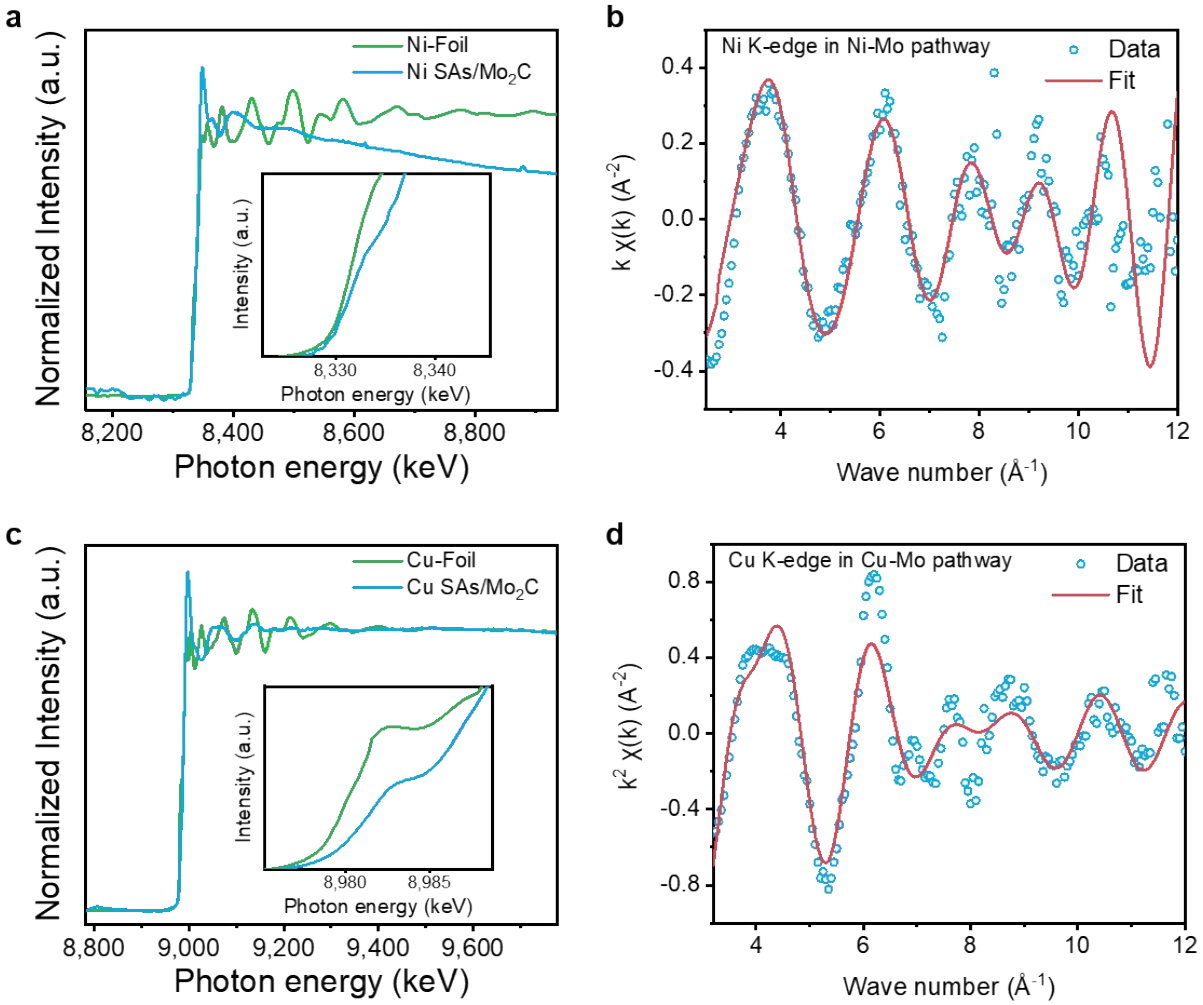

Figure S17. a, **c** XANES spectra of Ni K-edge and Cu K-edge in Ni SAs/Mo_2C (a) and Cu SAs/Mo_2C (c). insets are enlarged pre-edge parts. **b**, **d** First-shell fitting k^2-weighted Ni K-edge (b) and Cu K-edge (**d**) EXAFS spectra in K space by using Ni-Mo and Cu-Mo pathways. The fitting parameters was summarized in **Tables S6** and **S7**.

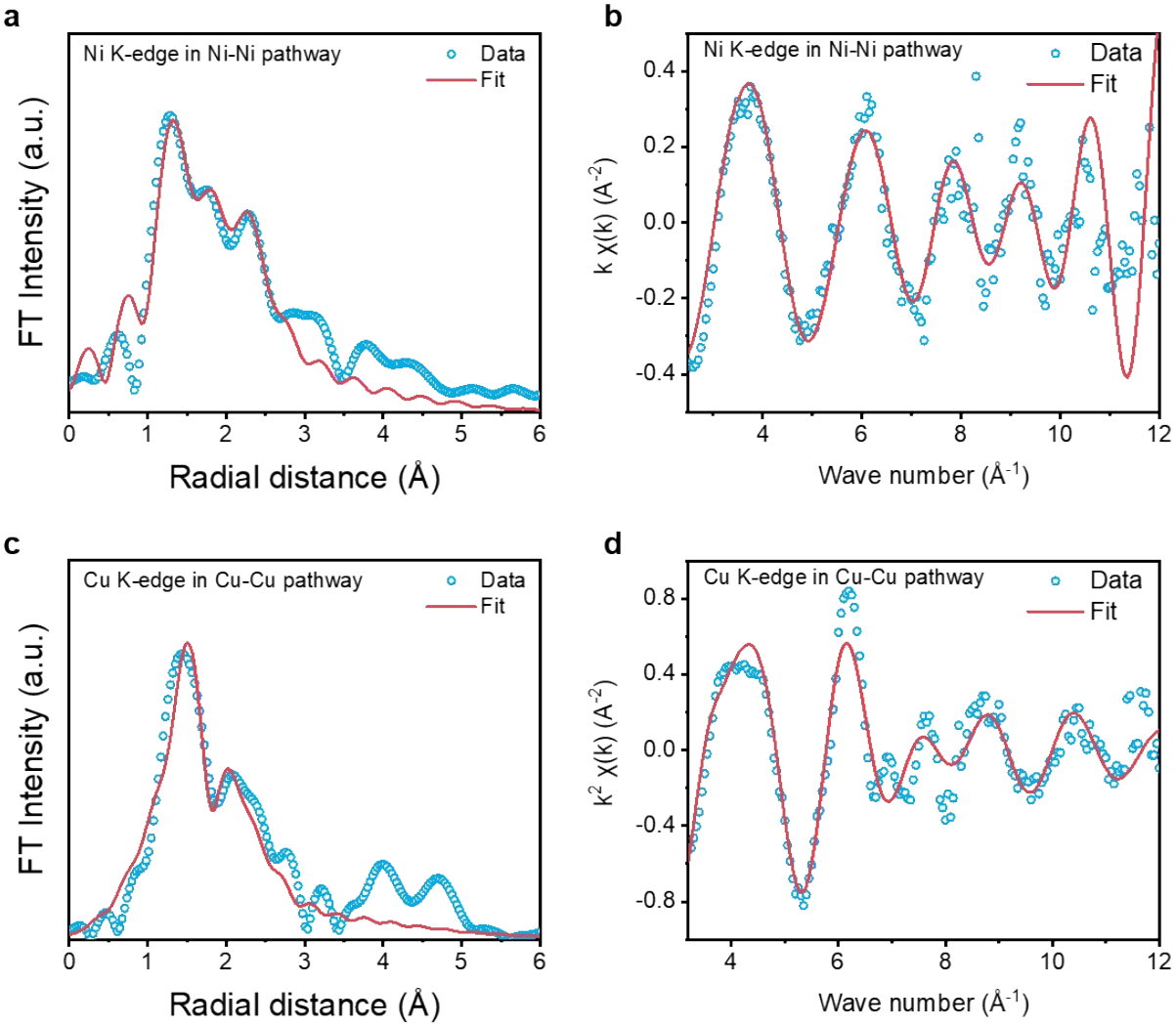

Figure S18. a, **c** First-shell fitting EXAFS spectra in R space of Ni K-edge and Cu K-edge in Ni SAs/Mo_2C (a) and Cu SAs/Mo_2C (c). **b**, **d** The corresponding first-shell fitting k^2-weighted Ni K-edge (b) and Cu K-edge (d) EXAFS spectra in K space by using Ni-Ni and Cu-Cu pathways. The fitting parameters was summarized in **Tables S6** and S**7**.

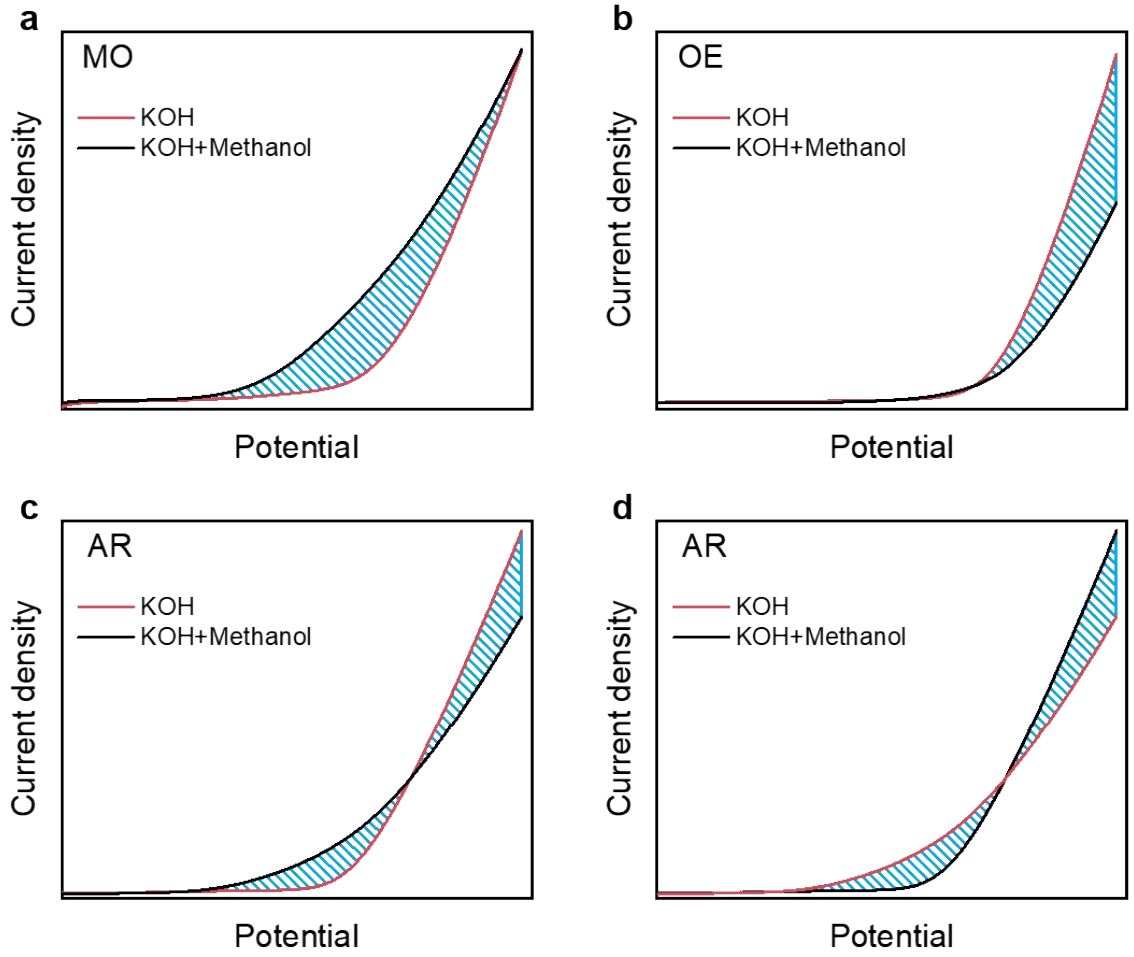

Figure S19. Schematic diagram of the three models associated with DIA method. **a**, **b** MO and OE models in which methanol oxidation and oxygen evolution are always preferable, respectively. **c**, **d** AR models in which methanol oxidation and oxygen evolution are alternating.

Table S1. Elemental content determined by ICP measurements. ND means "not detected".

Sample	Single atom metals (wt%)	Mo (wt%)	Zn (wt%)
Co-Mo/Zn BIFs	0.60	30.68	20.17
Co SAs/Mo_2C	1.78	85.72	ND
Ni-Mo/Zn BIFs	0.10	31.36	19.86
Ni SAs/Mo_2C	0.29	86.49	ND
Cu-Mo/Zn BIFs	1.32	30.37	20.52
Cu SAs/Mo_2C	3.92	84.74	ND

Table S2. The EXAFS fitting parameters for Co SAs/Mo_2C with a Co-Mo and Co-Co path.

	Path	R (Å)	N	E_0	σ^2 (Å^2)	R_f (%)
Co SAs/Mo_2C	Co-Mo	2.17	3	-16.881	0.0196	0.34
	Co-C	1.73	6	0.688	0.0189	
Co SAs/Mo_2C	Co-Co	2.29	8	54.289	0.0105	8.07
	Co-C	2.86	6	36.226	0.4509	

Table S3. A survey of the OER performances of most active oxides/hydroxides-based electrocatalysts from literatures in recent three years.

Literature	Materials	Catalyst loading (mg cm^{-2})	η@j=10 mA cm^{-2} (mV)	J at 1.6 V (mA cm^{-2})
This work	Co SAs/Mo_2C	1	270	49.7
Energy Environ. Sci., 2019,12, 684-692.	boronized NiFe alloy sheets	N/A	309 based ECSA	>90
Adv. Mater. 2017, 29, 1700017.	NiFe LDH-NS@DG	0.283	~300	>60
Adv. Mater. 2017, 29, 1701546.	CoFe LDHs	0.408	~320	>50
Nat. Commu. 2018, 9, 381.	CS-NiFeCu	N/A	180	>400
Nano Energy 2018, 43, 110-116.	CoO_x	0.5	306	45
Adv. Mater. 2019, 31, 1805658.	$Co_{1.8}Ni(OH)_{5.6}$@$Co_{1.8}NiS_{0.4}(OH)_{4.8}$	0.25	274	>40

Table S4. A survey of the OER performances of most active single atom electrocatalysts from literatures in recent three years.

Literature	Materials	Catalyst loading (mg cm^{-2})	η@j=10 mA cm^{-2} (mV)	J at 1.6 V (mA cm^{-2})
This work	Co SAs/Mo_2C	1	270	49.7
Nano Energy 2018, 50, 691-698.	CoN_4/NG	0.24	380	8
Nat. Catal. 2018, 1, 63-72.	Ni-NHGF	0.275	331	25
J. Am. Chem. Soc. 2017, 139, 1878-1884.	SNG-Co^{2+}	N/A	370	10
J. Mater. Chem. A 2018, 6, 6840-6846.	NiFe@g-C_3N_4/CNT	0.382	326	26
Nano Energy 2017, 41, 417-425.	CUMSs-ZIF-67	0.097	320	5.5
Chem 2018, 4, 285-297.	A-Ni@DG	0.262	270	44
ACS Catal. 2018, 8, 8961-8969.	NC-Co SA	1.35	360	12
Adv. Mater. 2019, 31, 1900592.	Co-POC	0.1	470	2.5
J. Am. Chem. Soc. 2017, 139, 3336-3339.	Co-C_3N_4/CNT	0.408	380	8

Table S5. A summary of free energy of each step on different models.

System	Mo_2C	Co SAs/Mo_2C	Co SAs/N-C	Pt(111)
ΔG_{H2O*}/eV	-1.35	-0.31	-0.17	0.17
ΔG_{H*}/eV	-1.79	-0.51	1.20	-0.39
ΔG_{HO*}/eV	-1.37	-1.24	0.99	0.85

Table S6. The EXAFS fitting parameters for Ni SAs/Mo_2C with a Ni-Mo and Ni-Ni path.

	Path	R (Å)	N	σ^2 (Å^2)	R_f (%)
Ni SAs/Mo_2C	Ni-Mo	2.27	3	-0.0070	0.80
	Ni-C	2.01	6	0.0076	
Ni SAs/Mo_2C	Ni-Ni	2.31	8	0.0122	0.85
	Ni-C	2.03	6	0.0099	

Table S7. The EXAFS fitting parameters for Cu SAs/Mo_2C with a Cu-Mo and Cu-Cu path.

	Path	R (Å)	N	σ^2 (Å^2)	R_f (%)
Cu SAs/Mo_2C	Cu-Mo	2.26	3	0.0082	6.52
	Cu-C	2.02	6	0.0042	
Cu SAs/Mo_2C	Cu-Cu	2.30	8	0.0124	6.77
	Cu-C	1.98	6	0.0044	